Mineralogical Magazine, April 2016, Vol. 80(2), pp. 311–324

Ferrivauxite, a new phosphate mineral from Llallagua, Bolivia

G. Raade[1,*], J. D. Grice[2] and R. Rowe[2]

[1] Natural History Museum, University of Oslo, PO Box 1172 Blindern, NO-0318 Oslo, Norway
[2] Canadian Museum of Nature, PO Box 3443, Station 'D', Ottawa, Ontario, K1P 6P4, Canada

[*Received 13 January 2015; Accepted 19 May 2015; Associate Editor: G. Diego Gatta*]

ABSTRACT

Ferrivauxite, ideally $Fe^{3+}Al_2(PO_4)_2(OH)_3 \cdot 5H_2O$, is an oxidized equivalent of vauxite, $Fe^{2+}Al_2(PO_4)_2(OH)_2 \cdot 6H_2O$, and forms oxidation pseudomorphs after that mineral. It occurs in association with sigloite and crandallite at the Llallagua tin deposit, Bolivia. It is triclinic, space group $P\bar{1}$, with $a = 9.198(2)$, $b = 11.607(3)$, $c = 6.112(2)$ Å, $\alpha = 98.237(9)$, $\beta = 91.900(13)$, $\gamma = 108.658(9)°$, $V = 609.7(5)$ Å^3, $Z = 2$. Strongest reflections of the powder X-ray diffraction pattern are [d_{obs} in Å(I_{obs})(hkl)]: 10.834(100)(010), 8.682(24)(100), 8.242(65)($\bar{1}$10), 6.018(28)(001), 5.918(23)(110), 5.491(30)($\bar{1}$20), 4.338(26)(200), 2.898 (32)(300). The structure was refined to $R1 = 0.0369$ for 3244 observed reflections. Twinning occurs on {010}. Ferrivauxite is isotypic with vauxite but with positional disorder of the Fe1 site and some of the oxygen sites. Disorder is also indicated by the infrared spectrum. One of the water molecules in vauxite is deprotonated in conjunction with the oxidation process and becomes a hydroxyl group.

Ferrivauxite is translucent to transparent, has a golden brown colour with a pale yellow-brown streak and vitreous lustre. It is brittle with an irregular fracture and shows no cleavage. The Mohs hardness is estimated to be ~3½ by comparison with vauxite. D(calc.) is 2.39 g cm^{-3} for the empirical formula $Fe^{3+}_{0.94}Mn_{0.01}Al_{1.98}P_{2.05}O_8(OH)_3 \cdot 5H_2O$, obtained by electron-microprobe analysis in wavelength dispersive spectroscopy mode. The mineral is optically biaxial negative with $\alpha = 1.589(1)$, $\beta = 1.593(1)$, $\gamma = 1.596(1)$; the refractive indices are higher than those of vauxite.

Keywords: ferrivauxite, new mineral, crystal structure, powder X-ray diffraction data, hydrogen bonding, infrared spectroscopy, Llallagua tin deposit, Bolivia.

Introduction

The new species ferrivauxite comes from the famous mineral locality Llallagua, Potosí, Bolivia (18°25′00″S 66°37′59″W, ~4000 m a.s.l.). It is a tin deposit and the type locality for four Fe-Al phosphate minerals (metavauxite, paravauxite, sigloite, vauxite) and jeanbandyite (Hyrsl and Petrov, 2006, and references therein).

Specimens were purchased in 1975 by the lead author and a collector friend, Mr Jan Haug, from the Mineralogical Research Company of San Jose, California. The golden brown mineral described here as ferrivauxite was identified on the labels as sigloite. It was subjected to powder X-ray diffraction (PXRD) and gave a pattern very close to that of vauxite. A mineral designated as paravauxite on the labels was identified as sigloite. According to Hyrsl and Petrov (2006), some so-called sigloite on the mineral market, originating from local Bolivian dealers, is in fact misidentified childrenite. Based on the material described here, it is likely that the mineral is actually ferrivauxite.

The mineral and name were approved by the Commission on New Minerals, Nomenclature and Classification (CNMNC) of the International Mineralogical Association (IMA 2014-003). The name ferrivauxite emphasizes that the mineral is an oxidized equivalent of vauxite. The latter was named in honour of George Vaux Jr (1863–1927), American lawyer and mineral collector. The main part of the holotype is housed in the collections of the Natural History Museum, University of Oslo, with catalogue number 43576. A small fragment of

* E-mail: gunn-ra@online.no
DOI: 10.1180/minmag.2015.079.7.15

the holotype is deposited in the collections of the Canadian Museum of Nature in Ottawa under catalogue number CMNMC 86850.

Occurrence

The Llallagua tin deposit is hosted by the Tertiary Salvadora conical porphyry stock, cropping out on Salvadora Mountain. The porphyry and porphyry breccia were heavily altered by silification, sericitization and tourmalinization before the ores were deposited in shear zones and fissures. Late-stage phosphates of Llallagua, including vauxite and the other Fe-Al phosphates, are considered to be of hydrothermal origin, formed from decomposition of fluorapatite which was the principal gangue mineral in some of the richest cassiterite veins (Hyrsl and Petrov, 2006). Vauxite, $Fe^{2+}Al_2(PO_4)_2(OH)_2{\cdot}6H_2O$, was described as a new species by Gordon (1923), occurring as sky-blue to Venetian-blue crystal crusts. Hyrsl and Petrov (2006) describe a find in 2003 of greenish-blue to bright-blue spheres of vauxite and were surprised to find that yellowish-brown to greenish-brown crystals from this new find were shown by PXRD to be vauxite as well. They attribute this colour change to be caused by "a very minor amount of oxidation". In the golden brown ferrivauxite described here, the oxidation has proceeded so far as to create a new species, the ferric analogue of vauxite.

The material investigated by us is in the form of porous and fragile crusts, 2–4 mm thick, with no attached substrate. Apparently they have formed along narrow fractures. The surface area of the specimens was several cm^2 before being divided for micromounting. Ferrivauxite is associated with colourless laths of sigloite, up to 1 mm long, which formed later than ferrivauxite. Sigloite is an oxidation product of paravauxite (Hurlbut and Honea, 1962). Consequently, considering the corresponding precursor minerals, paravauxite formed later than vauxite, which is consistent with the observation made by Gordon (1944). Botryoidal coatings of tiny, porous globules of crandallite, up to 25 μm in diameter, constitute the last-formed phase, growing preferentially on ferrivauxite (Fig. 1).

Physical and optical properties

Platy ferrivauxite crystals typically occur as radial aggregates (Fig. 1), up to 0.7 mm in size, and as crystals in parallel growth. Thin-bladed, swallow-tail twins are observed. Crystal habit is tabular on {010}; no other forms were determined. However, the precursor mineral vauxite is known to show the forms {010}, {1$\bar{1}$0}, {$\bar{1}\bar{1}$1}, {101}, {1$\bar{1}$1}, {$\bar{1}$01} and {1$\bar{4}$0} (Anthony *et al.*, 2000) which should also occur on ferrivauxite. Twinning on {010} is the same as for vauxite.

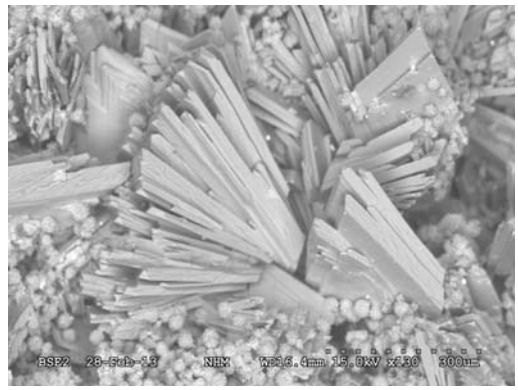

FIG. 1. SEM back-scatter electron image of typical fan-shaped aggregates of ferrivauxite, partially overgrown by globular crandallite.

Except for the golden brown colour, ferrivauxite has the same appearance as vauxite and forms oxidation pseudomorphs after that mineral. The streak is pale yellow-brown, the lustre is vitreous, and the diaphaneity is translucent to transparent. The mineral is non-fluorescent. The tenacity is brittle and the fracture is irregular. Cleavage and parting were not observed. The Mohs hardness is expected to be ~3½ by analogy with vauxite. Density determination was not attempted because the crystal aggregates are likely to trap air bubbles (Fig. 1). Furthermore, the compositional and structural differences between ferrivauxite and vauxite are so small that both have D(calc.) = 2.40 g cm^{-3} for the ideal compositions $Fe^{3+}Al_2(PO_4)_2(OH)_3{\cdot}5H_2O$ and $Fe^{2+}Al_2(PO_4)_2(OH)_2{\cdot}6H_2O$, respectively. D(calc.) = 2.39 g cm^{-3} for the empirical formula $Fe^{3+}_{0.94}Mn_{0.01}Al_{1.98}P_{2.05}O_8(OH)_3 \cdot 5H_2O$.

Ferrivauxite is biaxial negative with refractive indices $\alpha = 1.589(1)$, $\beta = 1.593(1)$, $\gamma = 1.596(1)$, measured at 589 nm. 2V(meas.) is 60(4)° from extinction curves and 76(5)° by the Kamb method; 2V(calc.) = 82°. Optic axis dispersion is distinct and inclined with r < v. Optical orientation: $X \wedge b = 14°$, $Y \wedge c = 4°$, $Z \wedge a = 0°$. The mineral is pale yellow in plane-polarized light. Pleochroism was not observed in any orientation on the spindle stage.

https://doi.org/10.1180/minmag.2015.079.7.15 Published online by Cambridge University Press

Chemical composition

Chemical analyses (17 on several different grains and aggregates) were carried out with a Cameca SX 100 electron microprobe (wavelength dispersive spectroscopy mode, using 15 kV, 5 nA and a 10 μm beam diameter). The elements Na, K, Ca, Mg and Si, which are reported as minor constituents of Fe-Al phosphates from Llallagua (Anthony *et al*., 2000), were included in the analyses but are below detection limits. All Fe is calculated as trivalent, although a small amount could possibly be divalent. Sigloite, the oxidized equivalent of paravauxite, has 2.76 wt.% FeO (Hurlbut and Honea, 1962). Water was not analysed because of difficulties in obtaining a sufficient amount of uncontaminated material; H_2O was calculated to bring the cation sum (Fe + Mn + Al + P) close to 5 for 13 H and 16 O atoms. Carbonate is not present according to the structure refinement and the infrared spectrum. Analytical data are given in Table 1. A low oxide total like the one in the table (97.64 wt.%) is not uncommon when analysing small grains embedded in an epoxy mount and especially in the case of thin and platy crystals.

The empirical formula (based on 16 O apfu) is, with rounding errors, $Fe^{3+}_{0.94}Mn_{0.01}Al_{1.98}P_{2.05}O_8(OH)_3 \cdot 5H_2O$. The simplified formula is $Fe^{3+}Al_2(PO_4)_2(OH)_3 \cdot 5H_2O$.

Ferrivauxite dissolves slowly in room temperature, dilute HCl and gives with ammonium thiocyanate a strong red colouration indicative of major Fe^{3+}, as does the associated sigloite. Ferrivauxite is stable in the vacuum of the scanning electron microscope, whereas sigloite turns white and crumbles.

The Gladstone-Dale compatibility index (Mandarino, 1981) $1-(K_p/K_c)$ is 0.020 (excellent) for the empirical formula $Fe^{3+}_{0.94}Mn_{0.01}Al_{1.98}P_{2.05}O_8(OH)_3 \cdot 5H_2O$ and 0.028 (excellent) for the ideal formula $Fe^{3+}Al_2(PO_4)_2(OH)_3 \cdot 5H_2O$.

Powder X-ray diffraction

Powder X-ray diffraction data for ferrivauxite (Table 2) were collected on a Bruker D8 Discover microdiffractometer (Cu$K\alpha$) with a Hi-Star detector and operated with *GADDS* software. The instrument was calibrated following the method described by Rowe (2009). Cell refinement was carried out using *CELREF* (Laugier and Bochu, 2003), and the calculated pattern was created in *POWDERCELL* (Kraus and Nolze, 1996). Unit-cell parameters refined from the indexed powder data are: $a = 9.200(2)$, $b = 11.621(2)$, $c = 6.101(1)$ Å, $\alpha = 98.36(2)$, $\beta = 91.86(2)$, $\gamma = 108.65(2)°$, $V = 609.3(2)$ Å^3.

Crystal structure

Structure solution and refinement

A single crystal (20 μm × 40 μm × 60 μm) was trimmed from a swallow-tail twin and mounted on a fully automated Bruker D8 three-circle diffractometer operated at 50 kV, 24 mA, with Mo$K\alpha$ radiation, multi-layer optics and an APEX-II CCD detector at a 5 cm distance from the crystal. This setup yields a very intense X-ray beam. Integrated intensities were collected up to $2\theta = 60.15°$, using 5 s frame counts and a frame width of 0.2°. The unit-cell parameters for the single crystal were refined using 99,999 (maximum allowable) indexed reflections: $a = 9.198(2)$, $b = 11.607(3)$, $c = 6.112(2)$ Å, $\alpha = 98.237(9)$, $\beta = 91.900(13)$, $\gamma =$

TABLE 1. Analytical data for ferrivauxite.

Constituent	Wt.%	Range	Std. dev.	Probe standard	Wt.%**
MnO	0.20	0.12–0.38	0.07	Pyrophanite	
Al_2O_3	22.43	21.79–23.47	0.52	Al_2O_3	23.13
Fe_2O_3	16.62	15.95–17.91	0.49	Fe metal	18.11
P_2O_5	32.32	31.04–34.35	0.90	Durango apatite	32.20
H_2O*	26.07				26.56
Total	97.64				100.00

*Calculated as explained in the text.
**Theoretical composition for $Fe^{3+}Al_2(PO_4)_2(OH)_3 \cdot 5H_2O$.

https://doi.org/10.1180/minmag.2015.079.7.15 Published online by Cambridge University Press

TABLE 2. Powder X-ray data for ferrivauxite (Cu*K*α radiation).

I_{obs}	I_{calc}*	d_{obs} (Å)	d_{calc} (Å)**	*hkl*
100	100	**10.834**	10.861	$0\bar{1}0$
24	19	**8.682**	8.686	$\bar{1}00$
65	33	**8.242**	8.227	$\bar{1}\bar{1}0$
28	23	**6.018**	6.014	$00\bar{1}$
23	12	**5.918**	5.904	$\bar{1}\bar{1}0$
3	5	5.679	5.671	$0\bar{1}\bar{1}$
30	20	**5.491**	5.484	$\bar{1}20$
21	9, 6	4.954	4.962, 4.929	$\bar{1}\bar{1}\bar{1}$, $01\bar{1}$
	1, 2		4.760, 4.755	$\bar{1}0\bar{1}$, $\bar{1}\bar{1}\bar{1}$
15	2, 8	4.574	4.585, 4.561	$\bar{2}\bar{1}0$, $\bar{1}\bar{1}\bar{1}$
16	7	4.406	4.407	$02\bar{1}$
26	12, 6	**4.338**	4.343, 4.301	200, $\bar{1}21$
3	1	4.119	4.114	$\bar{2}20$
3	1	4.045	4.046	120
2	<1	3.941	3.934	$\bar{1}\bar{1}1$
3	1	3.828	3.842	$\bar{1}21$
21	3, 4, 6, 1, 3	3.641	3.681, 3.671, 3.641,	$\bar{2}\bar{1}1$, $\bar{2}01$, $2\bar{1}0$,
			3.620, 3.612	030, $2\bar{1}\bar{1}$
22	4, 4, 6	3.378	3.388, 3.379, 3.355	$20\bar{1}$, $\bar{2}30$, $03\bar{1}$
10	2, 4	3.318	3.327, 3.305	$\bar{2}2\bar{1}$, $\bar{2}\bar{1}\bar{1}$
16	1, 1, 7, 3	3.039	3.063, 3.059, 3.040, 3.029	2–31, $\bar{3}10$, $\bar{1}3\bar{1}$, $0\bar{1}2$,
	1, 2		3.007, 2.995	002, $\bar{3}20$
20	5, 6	2.953	2.955, 2.952	$2\bar{1}\bar{1}$, 220
	1		2.919	$\bar{1}02$
32	4, 12, 1, 1	**2.898**	2.898, 2.895, 2.890, 2.874	$03\bar{1}$, 300, $\bar{1}3\bar{1}$, $\bar{1}40$
11	5, 1, 3, 1	2.851	2.854, 2.841, 2.836, 2.818	$\bar{1}\bar{1}2$, $\bar{2}31$, $0\bar{2}2$, $\bar{2}\bar{2}1$
22	1, 1, 1, 4,	2.755	2.783, 2.775, 2.772, 2.770,	$0\bar{1}2$, $\bar{3}1\bar{1}$, $1\bar{2}2$, 102,
	4, 3, 7		2.754, 2.742, 2.742	$1\bar{4}1$, $\bar{3}30$, $\bar{2}40$
3	2, 1	2.708	2.715, 2.699	040, $30\bar{1}$
2	1	2.679	2.678	$\bar{3}21$
6	3, 1	2.626	2.625, 2.609	$\bar{1}\bar{2}2$, $2\bar{4}1$
4	3	2.579	2.576	$\bar{2}02$
14	3, 2, 4, 2	2.535	2.537, 2.536, 2.533. 2.508	$\bar{2}12$, $1\bar{3}2$, 112, 221
3	3, 1	2.489	2.481, 2.477	$2\bar{2}2$, $2\bar{1}2$
3	1, 1	2.460	2.457, 2.454	$\bar{1}41$, $\bar{3}31$

2	2	2.424	2.415	$\bar{3}40$
6	1, 1, 2	2.380	2.380, 2.377, 2.379	202, $\bar{2}22$, 140
4	1, 1	2.333	2.335, 2.329	$\bar{0}41$, $\bar{1}32$
4	1, 1, 3	2.288	2.303, 2.292, 2.280	$\bar{3}41$, 150, $\bar{2}22$
6	1, 2, 3, 1	2.259	2.265, 2. 262, 2.246, 2.248	320, $\bar{2}50$, 122, $1\bar{4}2$
2	1, 1	2.216	2.219, 2.203	$\bar{1}32$, $0\bar{4}2$
4	2, 1, 1	2.180	2.188, 2.179, 2.172	212, 302, 400
2	1, 1	2.159	2.156, 2.151	$\bar{4}21$, $2\bar{4}2$
2	1, 1	2.131	2.131, 2.126	$\bar{2}31$, $3\bar{2}2$
11	3, 4, 1	2.101	2.100, 2.100, 2.095	$\bar{4}01$, $\bar{3}50$, 141
3	1	2.063	2.057	$\bar{4}40$
2	1	2.048	2.047	$\bar{2}32$
2	1	2.030	2.031	321
2	1, 2	1.990	2.005, 1.9899	$\bar{0}03$, $0\bar{2}3$
7	1, 1, 2, 1, 1	1.9659	1.9722, 1.9699, 1.9679, 1.9672, 1.9570	$\bar{1}52$, 132, 330, $\bar{2}22$, $3\bar{4}2$
2	2	1.9376	1.9387	$\bar{3}22$
	1		1.9182	103
4	1, 1, 1, 1	1.8999	1.9010, 1.8945, 1.8904, 1.8815	$\bar{1}60$, $2\bar{6}1$, $0\bar{3}3$, $\bar{2}03$
2	1	1.8645	1.8682	$0\bar{4}2$
2	1, 1, 1	1.8429	1.8501, 1.8404, 1.8354	$\bar{2}13$, $\bar{4}22$, $\bar{4}02$
5	1, 1, 1, 1, 1, 1	1.8121	1.8281, 1.8129, 1.8106, 1.8067, 1.8064, 1.8061	$\bar{3}60$, $\bar{1}33$, $\bar{5}10$, $3\bar{6}1$, $3\bar{5}2$, $4\bar{2}2$
4	3, 3	1.7903	1.7942, 1.7876	$\bar{3}31$, $0\bar{2}3$
4	1, 1	1.7713	1.7698, 1.7820	$\bar{3}32$, $\bar{4}32$
2	2	1.7510	1.7465	$5\bar{4}0$
2	1, 1, 1	1.7248	1.7342, 1.7320, 1.7244	$4\bar{4}2$, $1\bar{6}2$, $\bar{3}41$
3	1, 1, 2	1.6964	1.7024, 1.6940, 1.6897	322, $4\bar{0}2$, $4\bar{6}0$
2	1, 1	1.6682	1.6774, 1.6634	$0\bar{6}2$, $\bar{4}42$
2	1	1.6613	1.6596	$0\bar{6}1$
2	2	1.6540	1.6523	$\bar{4}22$
2	1	1.6410	1.6420	$\bar{4}52$
3	2, 1	1.5911	1.5914, 1.5907	$\bar{4}12$, $\bar{4}61$
3	1, 1, 1	1.5284	1.5357, 1.5317, 1.5313	$2\bar{7}2$, $\bar{4}62$, $\bar{4}32$
4	2, 1, 1	1.5197	1.5237, 1.5200, 1.5144	$0\bar{1}4$, $\bar{2}62$, $0\bar{2}4$
4	1, 2, 1	1.5033	1.5054, 1.5035, 1.5029	$\bar{1}62$, 004, $\bar{1}04$
1	1	1.4913	1.4869	$2\bar{6}3$
3	1, 1	1.4717	1.4773, 1.4759	422, 440

(continued)

https://doi.org/10.1180/minmag.2015.079.7.15 Published online by Cambridge University Press

TABLE 2. (*contd.*)

I_{obs}	I_{calc}*	d_{obs} (Å)	d_{calc} (Å)**	*hkl*
2	1, 2, 1, 1	1.4484	1.4491, 1.4477, 1.4449, 1.4429	062, $\underline{6}00$, $\underline{\overline{2}}62$, $\underline{6}\bar{5}0$
5	1	1.4390	1.4370	$\underline{2}\bar{8}0$
2	1, 1	1.4203	1.4258, 1.4207	$\underline{3}\bar{8}1$, $\underline{\bar{4}}62$
3	1, 1	1.4034	1.4099, 1.4045	$\underline{3}23$, $\underline{4}43$
2	1, 1	1.3846	1.3873, 1.3852	$\underline{6}\bar{2}2$, $\underline{2}04$
2	1	1.3727	1.3764	081

* Calculated from crystal-structure determination. With one exception, only reflections with intensities ≥1 are given. ** Calculated from PXRD cell refinement with a = 9.200(2), b = 11.621(2), c = 6.101(1) Å, α = 98.36(2), β = 91.86(2), γ = 108.65(2)°, V = 609.3(2) Å^3. Reflections used for cell refinement are underlined. The eight strongest observed peaks are in bold.

108.658(9)° and V = 609.7(5) Å^3; space group $P\bar{1}$, Z = 2. Standard deviations for cell parameters combine both random-errors and systematic errors.

Reduction of the intensity data, structure determination and structure refinement were performed with the *SHELXTL* (Sheldrick, 1990) package of computer programs. Data reduction included corrections for background, scaling and Lorentz-polarization factors. An empirical absorption correction (*SADABS*; Sheldrick, 1998) was applied. The merging R_{int} for the complete dataset (24,014 reflections) decreased from 0.0577 before the absorption correction to 0.041 after the absorption correction. Information on data collection and the final structure refinement is given in Table 3, atom coordinates and anisotropic displacement factors in Table 4 and selected interatomic distances in Table 5.

Structure description

The crystal structure of vauxite was described by Baur and Rama Rao (1968). The ferrivauxite

TABLE 3. Crystal data and information on data collection and final structure refinement for ferrivauxite.

Ideal unit-cell contents	$2[Fe^{3+}Al_2(PO_4)_2(OH)_3{\cdot}5H_2O]$
Space group	$P\bar{1}$
Unit-cell dimensions a, b, c (Å)	9.198(2), 11.607(3), 6.112(2)
α, β, γ (°)	98.237(9), 91.900(13), 108.658(9)
Unit-cell volume (Å^3)	609.7(5)
Crystal dimensions (μm)	20 × 40 × 60
Absorption coefficient μ (mm^{-1})	1.74
2θ range (°)	4.70–60.15
h, k, l ranges	–12 → 12, –16 → 16, –8 → 8
Measured reflections	7132
Unique reflections	3570
Observed reflections [$F > 4\sigma(F)$]	3244
R_{int} (%)	1.21
Refinement method	Full-matrix least-squares on F^2
Refined parameters	264
$R1$ and $wR2$ for observed reflections (%)	3.69, 10.59
Goodness of fit on F^2	1.032
Largest difference peak and hole (e Å^{-3})	+1.28, –1.05

https://doi.org/10.1180/minmag.2015.079.7.15 Published online by Cambridge University Press

TABLE 4. Fractional atom coordinates and anisotropic displacement factors (Å^2) for ferrivauxite.

Site	*x*/*a*	*y*/*b*	*z*/*c*	Occup.	U^{11}	U^{22}	U^{33}	U^{23}	U^{13}	U^{12}	U_{eq}/U_{iso}
Fe1	–0.00803(4)	–0.00400(4)	0.01400(6)	0.37195(17)	0.02867(6)	0.01567(4)	0.02780(7)	–0.00763(5)	–0.00588(5)	0.01113(4)	0.02447(4)
Fe2	0	½	0	0.9081(3)	0.01528(3)	0.01401(3)	0.01070(3)	0.00114(3)	–0.00236(3)	0.00480(3)	0.01350(2)
Al1	0.664077(13)	0.289967(11)	0.180452(19)	1	0.01282(4)	0.01718(4)	0.00884(4)	0.00268(4)	0.00202(4)	0.00643(3)	0.01250(3)
Al2	0	½	½	1	0.01335(6)	0.01220(6)	0.01228(6)	0.00203(5)	0.00529(5)	0.00487(5)	0.01234(4)
Al3	½	½	0	1	0.01238(6)	0.01914(6)	0.01196(6)	0.00383(5)	0.00270(5)	0.00810(5)	0.01361(4)
P1	0.986175(12)	0.265827(9)	0.209905(18)	1	0.01487(4)	0.01514(4)	0.01570(4)	–0.00047(3)	0.00121(3)	0.00632(3)	0.01521(2)
P2	0.311753(11)	0.638203(9)	0.292342(15)	1	0.01022(3)	0.01619(4)	0.00823(3)	0.00143(3)	0.00128(3)	0.00439(3)	0.01158(2)
O1	0.80893(3)	0.20632(3)	0.19308(5)	1	0.01440(11)	0.01571(11)	0.01910(12)	0.00206(10)	0.00094(10)	0.00506(9)	0.01647(7)
O2	0.03235(3)	0.33836(3)	0.01288(5)	1	0.01855(11)	0.02299(12)	0.01576(12)	0.00336(10)	0.00497(10)	0.00800(9)	0.01871(8)
O3	0.04129(3)	0.35356(3)	0.43002(5)	1	0.01788(11)	0.01711(11)	0.01389(11)	–0.00020(9)	–0.00048(10)	0.00812(8)	0.01604(7)
O4	0.06096(4)	0.16510(3)	0.19343(6)	1	0.02410(13)	0.01960(12)	0.03103(16)	–0.00319(12)	–0.00238(12)	0.01277(9)	0.02443(9)
O5	0.13624(3)	0.56831(3)	0.28774(5)	1	0.01035(10)	0.01891(11)	0.01277(11)	0.00123(9)	0.00130(9)	0.00264(9)	0.01466(7)
O6	0.63130(3)	0.28860(3)	0.47836(5)	1	0.01686(11)	0.02242(12)	0.00982(11)	0.00174(10)	0.00138(10)	0.00411(9)	0.01701(8)
O7	0.33182(3)	0.72630(3)	0.12475(5)	1	0.01980(12)	0.01801(11)	0.00949(10)	0.00256(9)	0.00216(10)	0.00574(9)	0.01582(7)
O8	0.39416(3)	0.54533(3)	0.23022(5)	1	0.01835(11)	0.02440(11)	0.01524(11)	0.00611(10)	0.00649(10)	0.01255(8)	0.01757(7)
O9	0.53190(3)	0.38375(3)	0.16442(5)	1	0.01677(10)	0.02424(11)	0.01359(11)	0.00709(9)	0.00619(9)	0.01162(8)	0.01649(7)
O10	0.84295(3)	0.45060(3)	0.24383(5)	1	0.01264(10)	0.01647(10)	0.01562(12)	–0.00036(9)	–0.00071(9)	0.00684(8)	0.01476(7)
O11A	0.77297(6)	0.96052(4)	0.13170(9)	0.6778(0)	0.02092(19)	0.01732(17)	0.0306(2)	–0.00098(16)	–0.00748(17)	0.00200(14)	0.02473(13)
O11B	0.64845(15)	1.01424(12)	0.0629(2)	0.2585(0)	0.02092(19)	0.01732(17)	0.0306(2)	–0.00098(16)	–0.00748(17)	0.00200(14)	0.02473(13)
O11C	0.6874(6)	0.9698(5)	0.2405(10)	0.0638(0)	0.02092(19)	0.01732(17)	0.0306(2)	–0.00098(16)	–0.00748(17)	0.00200(14)	0.02473(13)
O12	0.06435(8)	0.92461(6)	0.27270(12)	0.8430(15)	0.0641(4)	0.0536(3)	0.0552(3)	0.0042(3)	–0.0205(3)	0.0124(3)	0.0604(2)
O13	0.49873(4)	0.13556(3)	0.12886(6)	1	0.02270(15)	0.02096(13)	0.02551(15)	0.00472(12)	–0.00459(13)	–0.00252(12)	0.02545(9)
O14	0.69309(3)	0.62033(3)	0.14798(5)	1	0.01443(11)	0.02373(13)	0.02141(13)	0.00087(11)	0.00308(11)	0.00534(10)	0.02033(8)
O15A	0.4459(3)	0.9701(2)	0.3809(4)	0.1394(0)	0.0239(3)	0.0213(2)	0.0292(3)	0.0032(2)	0.0003(3)	0.0037(2)	0.02583(18)
O15B	0.3076(3)	0.9422(3)	0.3070(5)	0.1242(0)	0.0239(3)	0.0213(2)	0.0292(3)	0.0032(2)	0.0003(3)	0.0037(2)	0.02583(18)
O15C	0.37565(9)	0.95901(7)	0.34804(13)	0.4597(0)	0.0239(3)	0.0213(2)	0.0292(3)	0.0032(2)	0.0003(3)	0.0037(2)	0.02583(18)
O15D	0.43970(15)	1.08759(12)	0.4056(2)	0.2767(0)	0.0239(3)	0.0213(2)	0.0292(3)	0.0032(2)	0.0003(3)	0.0037(2)	0.02583(18)
O16	0.70850(5)	0.80455(5)	0.47551(9)	0.9446(13)	0.03343(18)	0.0517(2)	0.0422(2)	–0.0074(2)	–0.00690(18)	0.01858(16)	0.04311(14)
H9	0.4947(8)	0.3817(10)	0.3076(7)	1							0.080(3)
H10	0.8083(6)	0.5204(4)	0.2671(19)	1							0.085(3)
H12A	0.1715(4)	0.9287(9)	0.303(2)	0.84							0.089(3)
H12B	–0.0223(5)	0.9189(12)	0.3562(10)	0.84							0.089(3)
H13A	0.4944(11)	0.0767(4)	0.2264(8)	1							0.079(2)
H13B	0.4111(5)	0.1130(9)	0.0242(9)	1							0.079(2)
H14A	0.7777(5)	0.6485(8)	0.0626(9)	1							0.066(2)

(continued)

TABLE 4. (*contd.*)

Site	*x/a*	*y/b*	*z/c*	Occup.	U^{11}	U^{22}	U^{33}	U^{23}	U^{13}	U^{12}	U_{eq}/U_{iso}
H14B	0.7033(10)	0.6840(5)	0.2738(8)	1							0.066(2)
H16A	0.7362(10)	0.7756(6)	0.6063(7)	0.94							0.131(4)
H16B	0.7392(18)	0.8816(4)	0.4065(11)	0.94							0.131(4)

structure is isotypic and is illustrated in Fig. 2. There are two Fe sites, three Al sites and two P sites (Table 4), Fe and Al occurring in six-fold coordination (Table 5). The Fe1 atom, situated at the origin in vauxite, is positionally disordered in ferrivauxite with an Fe1–Fe1 separation of 0.2392(7) Å, which is too small for independent refinement. The Fe1 site shown in Table 4 refined to an occupancy factor of 0.37.

Alternating Fe2 and Al2 octahedra share edges to form chains parallel to [001]. Vertex-linked chains along [001] of alternating P2 tetrahedra and Al1 octahedra are connected to the octahedral chain through vertices bound on two opposite sides. The resulting triple chains are linked to P1 tetrahedra which share vertices with the Al1, Al2 and Fe2 octahedra, forming decorated triple chain units which are in turn interconnected laterally via vertex-linked Al3 octahedra in the [100] direction and Fe1 octahedra in the [010] direction.

Of the five water molecules present, two, O15 and O16, are situated in [001] channels of the structure, where O15 is significantly disordered and O16 is almost fully occupied (occupancy 0.94) (Table 4). The other three, O12, O13 and O14, are ligands of the Fe1, Al1 and Al3 octahedra, respectively, and while O13 and O14 are fully occupied, O12 has a slightly reduced occupancy (0.84). These five water molecules are equivalent to those occurring in vauxite. The sixth water molecule in vauxite is analogous to O11 in ferrivauxite and like the O12 water molecule is bonded to Fe1. The O11 water molecule in ferrivauxite is thus the obvious candidate for deprotonation in conjunction with the oxidation process, with the O12 water molecule remaining relatively intact although with a slightly reduced occupancy. O11 in ferrivauxite has then become a hydroxyl group where, as might be expected due to the strongly disordered nature of this oxygen atom (Table 4), no hydrogen atoms were detected in the difference map. The remaining two hydroxyl groups, O9 and O10, are both fully occupied, where O9 is common to the Al1 and Al3 octahedra whereas O10 is common to the Fe2, Al2 and Al1 octahedra.

Moore and Araki (1974) have pointed out a structural similarity between montgomeryite, $Ca_4MgAl_4(PO_4)_6(OH)_4{\cdot}12H_2O$ and vauxite. The two minerals possess topologically and geometrically equivalent vertex-linked Al–O octahedral chains. The octahedra are connected through OH ligands. These chains and associated PO_4 tetrahedra can be written $[Al_4(OH)_4(PO_4)_6]^{10-}$ for montgomeryite and $[Al_4(OH)_4(H_2O)_4(PO_4)_4]^{4-}$

https://doi.org/10.1180/minmag.2015.079.7.15 Published online by Cambridge University Press

TABLE 5. Selected interatomic distances (Å) for ferrivauxite.

Fe1–O4	1.9995(7)	Al1–O7	1.8507(7)
–O4	2.0095(7)	–O6	1.8568(7)
–O12	2.0707(10)	–O9	1.8820(5)
–O11A	2.0965(8)	–O1	1.8883(5)
–O12	2.2126(10)	–O13	1.9202(5)
–O11A	2.2979(8)	–O10	2.0303(5)
<Fe1–O>	2.1145	<Al1–O>	1.9047
Fe2–O2	2.0031(6) x2	Al2–O3	1.8524(5) x2
–O5	2.0274(6) x2	–O5	1.9102(5) x2
–O10	2.1198(6) x2	–O10	1.9823(6) x2
<Fe2–O>	2.0501	<Al2–O>	1.9150
P1–O4	1.5282(5)	Al3–O8	1.8468(5) x2
–O3	1.5284(5)	–O9	1.8811(5) x2
–O1	1.5471(5)	–O14	1.9667(5) x2
–O2	1.5604(5)	<Al3–O>	1.8982
<P1–O>	1.5410		
P2–O6	1.5118(5)	Fe1–Fe1	0.2392(7)
–O8	1.5182(5)		
–O7	1.5234(5)		
–O5	1.5549(4)		
<P2–O>	1.5271		

for vauxite and ferrivauxite. The zigzag chain Al2–Al1–Al3–Al1–Al2 is seen to stretch along the [100] direction in Fig. 2. Olmsteadite, $KFe^{2+}_2(Nb, Ta)(PO_4)_2O_2 \cdot 2H_2O$, contains the same kind of structural unit, in this case involving (Nb,Ta)–O octahedra as well (Moore *et al*., 1976).

The result of bond-valence calculations is shown in Table 6. Calculated bond-valence sums for the two phosphate groups and the three Al octahedra are satisfactory. Fe2 calculates to 2.76 vu; the slightly low value could be caused by the presence of minor Fe^{2+}. Splitting of the Fe1 and O11 sites, low occupancy (0.68) of O11A and distortion of the Fe1 octahedron (Table 5) preclude a bond-valence calculation for Fe1. Taking into account the contributions from hydrogen bonds, most of the oxygen atoms in Table 6 have satisfactory bond-valence sums. The O1 atom with 1.70 vu is undersaturated, and there is probably a contribution from a hydrogen bond involving the disordered O15 water molecule. The valence sum of 2.38 vu for O4 may be related to the splitting of Fe1 of which O4 is a ligand.

The *SHELXL* program enumerates a number of possible hydrogen bonds in ferrivauxite, the large number obviously being due to the positional disorder of the O11 and O15 atoms. In Table 7, nine specified hydrogen bonds are shown and compared to the hydrogen-bonding scheme in the unoxidized vauxite structure (Baur and Rama Rao, 1968). Three additional hydrogen bonds involving split O11 and O15 sites are included in the table. Most of the hydrogen bonds remain unchanged, but the situation is complicated by the splitting of O11 and O15 in ferrivauxite and the disordering of the Fe1 cation off its ideal position at the origin. The O9–H9 hydroxyl group does not form a hydrogen bond, as was also concluded by Baur and Rama Rao (1968). It should be emphasized that no proton sites were determined by Baur and Rama Rao (1968), their study being based on precession photographs, and the hydrogen bonds were assigned from O–O distances.

Infrared spectroscopy

Ferrivauxite was subjected to Fourier transform infrared spectroscopy (FTIR). The sample was positioned on a diamond anvil microsample cell and analysed using a Hyperion 2000 microscope equipped with a mid-band MCT detector, which

https://doi.org/10.1180/minmag.2015.079.7.15 Published online by Cambridge University Press

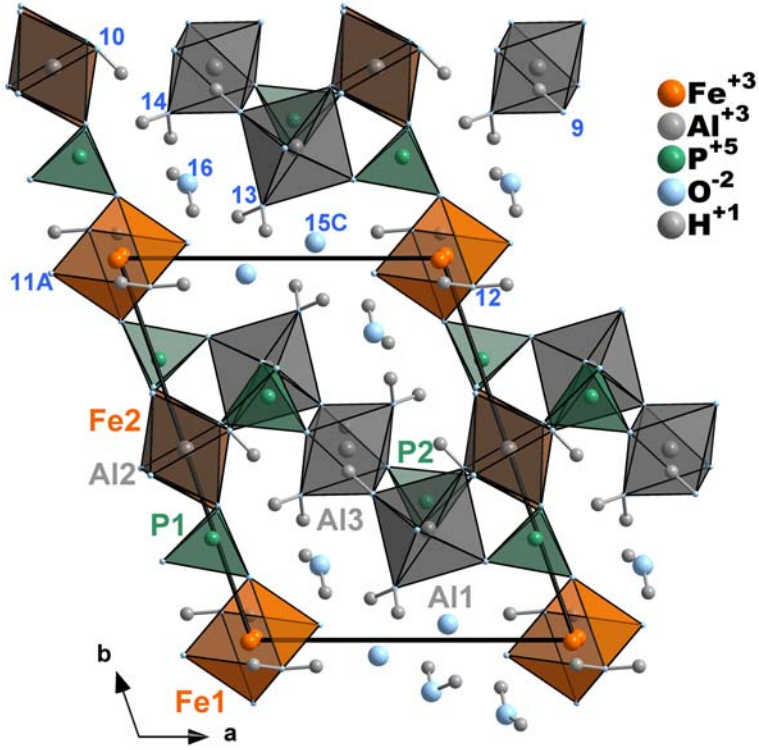

FIG. 2. The crystal structure of ferrivauxite viewed down [001]. The split Fe1 site is situated close to the origin whereas the Fe2 octahedra are almost hidden below Al2 octahedra midway along the *b* cell edge. Oxygen atoms forming hydroxyl groups or water molecules are numbered. The unit cell is indicated.

was interfaced to a Bruker Tensor 27 spectrometer. The spectrum was acquired in the 4000 to 570 cm^{-1} range by co-adding 200 scans and is shown in Fig. 3.

A rather poor resolution of absorption bands in the spectrum of ferrivauxite, as compared to that of vauxite from the type locality Llallagua (Chukanov, 2014), is caused by structural disorder in ferrivauxite as discussed above. Bands in the range from 1000 to 1200 cm^{-1} (at 1007, 1087 and 1125 cm^{-1}) can be assigned to asymmetric P–O stretching vibrations of PO_4 tetrahedra. The presence of a shoulder between 900 and 1000 cm^{-1} is due to symmetric P–O stretching vibrations of PO_4 tetrahedra and reflects distortions of the tetrahedra. This is in accordance with the variable P–O interatomic distances shown in Table 5. The weak bands in the region from 2000 to 2500 cm^{-1} correspond to very strong hydrogen bonds and can most probably be assigned to an acid HPO_4^{2-} group. Chukanov (pers. comm. 2014) has pointed out that a partial reversible proton transfer from water molecules to phosphate anions according to the dynamic equilibrium $H_2O + PO_4^{3-} \leftrightarrow OH^- + HPO_4^{2-}$, shifted towards the left side, is possible. This would be in agreement with the distortions of the PO_4 tetrahedra. It should be noted that the PO_4 tetrahedra in vauxite have very uniform P–O bond lengths, varying from 1.52 to 1.54 Å in the case of P1 and from 1.52 to 1.53 Å for P2 (Baur and Rama Rao, 1968).

The band at 1638 cm^{-1} corresponds to bending vibrations of H_2O molecules. The broad absorption region with a maximum at 3348 cm^{-1} is due to O–H stretching vibrations from rather strong hydrogen bonds in OH groups and H_2O molecules. The narrow band at 3640 cm^{-1} is caused by an OH group forming a very weak hydrogen bond. It also appears at 3645 cm^{-1} in the spectrum of vauxite (Chukanov, 2014). The plot of O–H stretching frequency versus O–H···O distance in Libowitzky (1999) does not allow derivation of reliable distances for such high frequencies. The maximum absorption at 3348 cm^{-1} corresponds

https://doi.org/10.1180/minmag.2015.079.7.15 Published online by Cambridge University Press

TABLE 6. Bond-valence analysis for ferrivauxite. Values are expressed in valence units (vu).

	Fe1	Fe2	Al1	Al2	Al3	P1	P2	H9	H10	H14A	H14B	H16A	H16B	Sum
O1			0.53			1.17								1.70
O2		0.52↓				1.13				0.21				1.86
O3				0.58↓		1.23								1.81
O4	0.52					1.23						0.12		2.38
	0.51													
O5		0.48↓		0.50↓			1.14							2.12
O6			0.57				1.28							1.85
O7			0.58				1.24							1.82
O8					0.59↓		1.26							1.85
O9			0.54		0.54↓			1.00						2.08
O10		0.38↓	0.36	0.41↓					0.86					2.01
O13			0.48											
O14					0.43↓				0.14	0.79	0.78			2.14
O16											0.22	0.88	0.89	1.99
Sum	—	2.76	3.06	2.98	3.12	4.76	4.92	1.00	1.00	1.00	1.00	1.00	1.00*	

Bond-valence parameters are from Brese and O'Keeffe (1991). Hydrogen bond strengths are from the bond-valence–bond-length correlation for H···O bonds in Brown and Altermatt (1985). The positionally disordered anions O11 and O15 are omitted, as well as the partially occupied O12 anion. O11 and O12 are ligands of the Fe1 octahedron; O15 belongs to a water molecule in [001] channels.
↓ is a short-hand notation for x2↓ multiplicity. * includes 0.11 vu from H16B···O11A.

TABLE 7. Selected hydrogen bonds in ferrivauxite.

D–H···A	d(D–H)	d(H···A)	>DHA	d(D→A)	d(D→A)*
O10–H10···O14	0.955(5)	1.994(7)	148.5(9)	2.8527(7)	2.86
O12–H12A···O15C	0.981(5)	1.800(4)	171.5(9)	2.7745(13)	2.82
O12–H12B···O11A	0.950(6)	2.502(9)	109.7(6)	2.9603(11)	2.91 (→O2)
O13–H13A···O15A	0.961	1.622	167.2	2.569	
O13–H13A···O15C	0.962(5)	1.733(6)	145.7(9)	2.5843(10)	2.60
O13–H13A···O15B	0.961	2.048	129.4	2.760	
O13–H13B···O11C	0.954	1.806	149.3	2.671	
O13–H13B···O11A	0.954(5)	1.799(5)	165.3(8)	2.7330(8)	2.72
O14–H14A···O2	0.947(5)	1.787(5)	152.7(8)	2.6643(7)	2.61
O14–H14B···O16	0.966(5)	1.715(5)	172.6(7)	2.6758(9)	2.71
O16–H16A···O4	0.967(6)	2.059(8)	130.3(6)	2.7834(9)	2.74
O16–H16B···O11A	1.006(5)	2.013(7)	149.0(5)	2.9207(10)	2.82

D: donor oxygen, A: acceptor oxygen, d: distance in Å, >: angle in °.
* O–O distance in vauxite (Baur and Rama Rao, 1968).

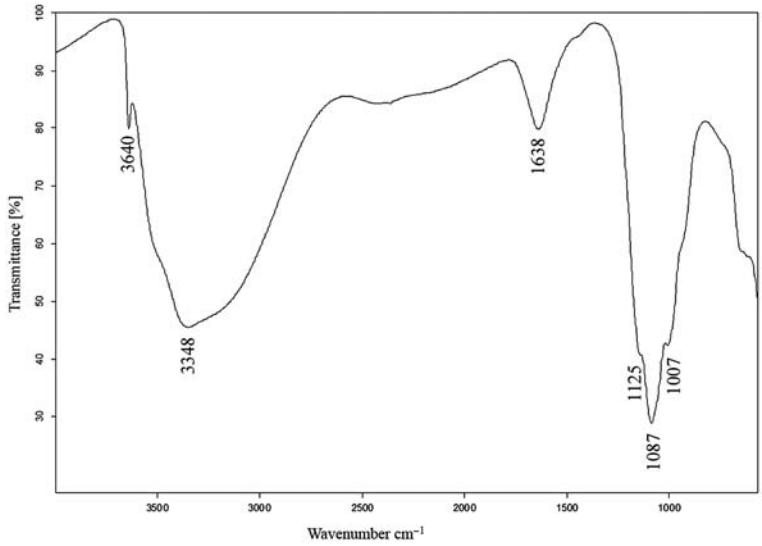

FIG. 3. FTIR spectrum of ferrivauxite.

roughly to an O–O distance of 2.76 Å, but the scatter of data points around the curve is relatively large. Several O–O distances of this magnitude are found in Table 7.

Ferrivauxite/vauxite versus sigloite/ paravauxite

The oxidation of vauxite to ferrivauxite is similar to the oxidation of paravauxite to sigloite. The crystal structure of sigloite, refined to $R = 5.3\%$, was described by Hawthorne (1988). The single Fe site at the origin in paravauxite is positionally disordered in sigloite, as are three of the O sites, two of them belonging to the Fe octahedron and the third to an H_2O group that is not bonded to any cation. Hawthorne (1988) concluded that the oxidation mechanism involves one of the H_2O groups bonded to Fe^{3+} becoming an OH group, and that "there must be considerable local

https://doi.org/10.1180/minmag.2015.079.7.15 Published online by Cambridge University Press

TABLE 8. Comparative data for ferrivauxite and vauxite.

Mineral	Ferrivauxite	Vauxite*
Formula	$Fe^{3+}Al_2(PO_4)_2(OH)_3 \cdot 5H_2O$	$Fe^{2+}Al_2(PO_4)_2(OH)_2 \cdot 6H_2O$
Space group	$P\bar{1}$	$P\bar{1}$
Cell data		
a (Å)	9.198	9.142
b (Å)	11.607	11.599
c (Å)	6.112	6.158
α (°)	98.237	98.29
β (°)	91.900	91.93
γ (°)	108.658	108.27
V (Å^3)	609.7	611.4**
Z	2	2
Strongest reflections	10.834 (100)	10.85 (100)
of PXRD pattern	8.242 (65)	5.908 (12)
d_{obs} in Å (I_{obs})	6.018 (28)	5.457 (20)
	5.918 (23)	3.045 (10)
	5.491 (30)	2.881 (12)
	4.338 (26)	2.596 (12)
	2.898 (32)	
Optical data		
α	1.589	1.551
β	1.593	1.555
γ	1.596	1.562
$2V_{calc}$ (°)	–82	+75**
Colour	Golden brown	Sky blue to Venetian blue

* Data from Anthony *et al*. (2000). ** Calculated for the present paper.

rearrangements in order for the local bond-valence requirements of all the ligand oxygens to be satisfied". Hawthorne (1988) has presented a detailed account of the ten local hydrogen-bond configurations that are possible around the split Fe atom in sigloite. Although complicated in detail, this is feasible for the sigloite structure because the O7 and O8 oxygen atoms are split into only two positions. In the ferrivauxite structure, O11 and O15 are split into three and four sites, respectively. The complex hydrogen-bonding network in paravauxite has been unravelled by Gatta *et al*. (2014), based on a single-crystal neutron diffraction study. Two of the proton sites are split, forming mutually exclusive subsite pairs only 0.4 to 0.6 Å apart.

The oxidation of paravauxite to sigloite involves shrinkage of the Fe octahedron, as could be expected. The mean Fe–O bond distance is 2.113 Å in paravauxite according to Baur (1969) and 2.123 Å according to Gatta *et al*. (2014), compared to 2.019 or 2.039 Å in sigloite, depending on whether the O7A or O7B atoms are considered. In ferrivauxite, the mean Fe–O bond length of the Fe2 octahedron is 2.0501 Å (Table 5), compared to 2.14 Å in vauxite (Baur and Rama Rao, 1968). However, the mean Fe–O bond length of 2.1145 Å for the Fe1 octahedron in ferrivauxite seems to be too high for trivalent iron, although it is smaller than the 2.18 Å mean bond distance in vauxite. Two very long Fe–O bonds, Fe1–O12 and Fe1–O11A are responsible for this larger than expected mean bond length. The other Fe1–O bonds are within the normal range for Fe^{3+}–O bonds. Positional disorder at the Fe1 and O11 sites in combination with lowered occupancies of O11 and O12 are disturbing factors when discussing bond distances and bond-valence calculation of the Fe1 octahedron in ferrivauxite.

Comparative data for ferrivauxite and vauxite are shown in Table 8. The increased refractive indices of ferrivauxite compared to those of vauxite should be noted. The situation is similar for sigloite and paravauxite.

https://doi.org/10.1180/minmag.2015.079.7.15 Published online by Cambridge University Press

Acknowledgements

Frédéric Hatert performed initial single-crystal investigations on the new mineral. We are indebted to Nikita Chukanov for commenting on the infrared spectrum, which was kindly recorded by Elizabeth Moffat of the Canadian Conservation Institute. Assistance with the EMP analyses by Muriel Erambert is appreciated. The SEM image was captured by Harald Folvik. The authors thank Frank Hawthorne, University of Manitoba, for the use of his four-circle diffractometer and Mark Cooper, University of Manitoba, for technical assistance. Peter Leverett, Anthony Kampf and an anonymous reviewer provided very detailed and helpful comments that have improved the paper.

References

Anthony, J.W., Bideaux, R.A., Bladh, K.W. and Nichols, M.C. (2000) *Handbook of Mineralogy. Volume IV. Arsenates, Phosphates, Vanadates*. Mineral Data Publishing, Tucson, pp. 625.

Baur, W.H. (1969) The crystal structure of paravauxite, $Fe^{2+}Al_2(PO_4)_2(OH)_2(OH_2)_6{\cdot}2H_2O$. *Neues Jahrbuch für Mineralogie, Monatshefte*, 430–433.

Baur, W.H. and Rama Rao, B. (1968) The crystal structure and the chemical composition of vauxite. *American Mineralogist*, **53**, 1025–1028.

Brese, N.E. and O'Keeffe, M. (1991) Bond-valence parameters for solids. *Acta Crystallographica*, **B47**, 192–197.

Brown, I.D. and Altermatt, D. (1985) Bond-valence parameters obtained from a systematic analysis of the inorganic crystal structure database. *Acta Crystallographica*, **B41**, 244–247.

Chukanov, N.V. (2014) *Infrared Spectra of Mineral Species: Extended Library.* Springer-Verlag GmbH, Dordrecht – Heidelberg – New York – London. 1716 pp.

Gatta, G.D., Vignola, P. and Meven, M. (2014) On the complex H–bonding network in paravauxite, $Fe^{2+}Al_2(PO_4)_2(OH)_2{\cdot}8H_2O$: A single-crystal neutron diffraction study. *Mineralogical Magazine*, **78**, 841–850.

Gordon, S.G. (1923) Vauxite and paravauxite, two new minerals from Llallagua, Bolivia. *Proceedings of the Academy of Natural Sciences of Philadelphia*, **75**, 261–267.

Gordon, S.G. (1944) The mineralogy of the tin mines of Cerro de Llallagua, Bolivia. *Proceedings of the Academy of Natural Sciences of Philadelphia*, **96**, 279–359.

Hawthorne, F.C. (1988) Sigloite: the oxidation mechanism in $[M_2^{3+}(PO_4)_2(OH)_2(H_2O)_2]^{2-}$ structures. *Mineralogy and Petrology*, **38**, 201–211.

Hurlbut Jr, C.S. and Honea, R. (1962) Sigloite, a new mineral from Llallagua, Bolivia. *American Mineralogist*, **47**, 1–8.

Hyrsl, J. and Petrov, A. (2006) Famous mineral localities: Llallagua, Bolivia. *Mineralogical Record*, **37**, 117–162.

Kraus, W. and Nolze, G. (1996) *POWDERCELL* – a program for the representation and manipulation of crystal structures and calculation of the resulting X-ray powder patterns. *Journal of Applied Crystallography*, **29**, 301–303.

Laugier, J. and Bochu, B. (2003) *LMGP Suite of Programs for the Interpretation of X-ray Experiments.* ENSP/Laboratoire des Matériaux et du Génie Physique, BP 46. 38042 Saint Martin d'Hères, France.

Libowitzky, E. (1999) Correlation of O–H stretching frequencies and O–H···O hydrogen bond lengths in minerals. *Monatshefte für Chemie*, **130**, 1047–1059.

Mandarino, J.A. (1981) The Gladstone–Dale relationship: Part IV. The compatibility concept and its application. *The Canadian Mineralogist*, **19**, 441–450.

Moore, P.B. and Araki, T. (1974) Montgomeryite, $Ca_4Mg(H_2O)_{12}[Al_4(OH)_4(PO_4)_6]$: Its crystal structure and relation to vauxite, $Fe_2^{2+}(H_2O)_4[Al_4(OH)_4(H_2O)_4(PO_4)_4]\cdot 4H_2O$. *American Mineralogist*, **59**, 843–850.

Moore, P.B., Araki, T., Kampf, A.R. and Steele, I.M. (1976) Olmsteadite, $K_2Fe_2^{2+}[Fe_2^{2+}(Nb,Ta)_2^{5+}O_4(H_2O)_4(PO_4)_4]$, a new species, its crystal structure and relation to vauxite and montgomeryite. *American Mineralogist*, **61**, 5–11.

Rowe, R. (2009) New statistical calibration approach for Bruker AXS D8 Discover microdiffractometer with Hi-Star detector using GADDS software. *Powder Diffraction*, **24**, 263–271.

Sheldrick, G.M. (1990) *SHELXTL, a crystallographic computing package, revision 4.1.* Siemens Analytical Instruments, Inc., Madison, Wisconsin, USA.

Sheldrick, G.M. (1998) *SADABS User Guide.* University of Göttingen. Göttingen, Germany.